LA-UR-94- 4386

Conf-9405204--3

Los Alamos National Laboratory is operated by the University of California for the United States Department of Energy under contract W-7405-ENG-36.

TITLE: Complex Scattering Dynamics and the Quantum Hall Effect

AUTHOR(S): S. A. Trugman

SUBMITTED TO: Proceedings of the CNLS Conference: "Quantum Complexity in Mesoscopic Systems", 1994

Los Alamos

Los Alamos National Laboratory
Los Alamos, New Mexico 87545

FORM NO. 836 R4
ST. NO. 2629 5/81

DISCLAIMER

DISCLAIMER

Portions of this document may be illegible in electronic image products. Images are produced from the best available original document.

Complex Scattering Dynamics and the Quantum Hall Effect

S. A. Trugman

Theoretical Division MS-B262, Los Alamos National Laboratory, Los Alamos, NM 87545

(December 16, 1994)

Abstract

We review both classical and quantum potential scattering in two dimensions in a magnetic field, with applications to the quantum Hall effect. Classical scattering is complex, due to the approach of scattering states to an infinite number of dynamically bound states. Quantum scattering follows the classical behavior rather closely, exhibiting sharp resonances in place of the classical bound states. Extended scatterers provide a quantitative explanation for the breakdown of the QHE at a comparatively small Hall voltage as seen by Kawaji et al., and possibly for noise effects.

I. INTRODUCTION

Reviews and collected papers on the quantum Hall effect can be found in Refs. [1–3]. The quantum Hall effect occurs when electrons are confined to two dimensions and placed in a strong magnetic field. The Hamiltonian is:

$$H = \frac{1}{2m}\sum_j (\vec{p}_j - \frac{e\vec{A}_j}{c})^2 + \sum_j V_R(\vec{r}_j) + \sum_{j<k} v_{12}(|\vec{r}_j - \vec{r}_k|) \; + \; [-e\vec{E}\cdot\sum_j \vec{r}_j], \tag{1.1}$$

where the magnetic field $\vec{B} = \vec{\nabla}\times\vec{A} = B\hat{z}$ and $\vec{r}_j = (x,y)$. The first term is the electron kinetic energy in the presence of a magnetic field. The second is a random potential, due perhaps to impurities. The third term is the repulsive interaction between electrons. The final term is added to study the linear and nonlinear response to a Hall electric field $\vec{E}$.

The fractional quantum Hall effect (FQHE) has plateaus of the Hall conductivity $\sigma_{xy} = (p/q)\ e^2/h$, where p and q are integers. It is a many-body problem in which the first and third terms in Eq. (1.1) are most important. The FQHE will not be discussed in this paper.

The integer quantum Hall effect has plateaus of the Hall conductivity at integer multiples of e^2/h. Most of the essential physics of the IQHE is captured by the one-body problem with the v_{12} term omitted. That is the approach taken here. Note that the random potential V_R cannot be omitted, even as a first approximation. Without V_R, the problem is simple to solve exactly using a Lorentz boost to a moving frame, and the plateaus in the Hall conductivity disappear.

For the IQHE then, perhaps the most basic question one could ask is: *"How does potential scattering happen in a magnetic field?"* As we discuss below, potential scattering in a magnetic field is quite complicated, and not completely understood. This question is often bypassed in the theory of the IQHE. Laughlin, for example, has given an elegant gauge invariance argument for the quantization of the Hall conductivity [4]. This argument cannot, however, explain what happens to σ_{xy} or σ_{xx} off of a plateau or at nonzero temperature or frequency. It also cannot explain nonlinear response, including the breakdown of the QHE, or noise or fluctuation effects. To deal with these questions, one must answer the basic question about scattering in a magnetic field. We first consider classical potential scattering in a magnetic field, and then quantum scattering.

Most of this article is a review. The quantitative comparison to breakdown experiments (Section V) has not appeared elsewhere.

II. CLASSICAL POTENTIAL SCATTERING

In zero magnetic field, scattering from a convex object is trivial. Trajectories either collide once with the object, or miss it entirely (see Fig. 1).

In a nonzero magnetic field perpendicular to the plane, a Hall electric field must also be present. Otherwise, a particle far from the potential will simply circle in a closed cyclotron

orbit, and never encounter the potential. The Hall electric field is taken to be in the $\hat{y}$ direction in this article.

Scattering in a magnetic field appears to divide into two cases, (1) scattering from a smooth, slowly varying potential, and (2) scattering from a rapidly varying potential. In the first case, scattering is tame. The guiding center of the incident particle's cyclotron orbit nearly follows an equipotential surface. The particle detours around the scatterer, and emerges with almost the same y guiding center coordinate that it entered with (see Fig. 2). The only important effect of the scatterer is that the outgoing particle reaches a given x coordinate at an earlier time than it would have for $V = 0$. Complicated dynamics can occur only if the trajectory approaches a saddle point. Scattering from a smooth potential has been discussed by several authors [5–8].

Scattering from an abrupt potential is more complicated. In contrast to scattering from a very smooth potential, the trajectory may encircle the scatterer many times before it escapes. The outgoing y guiding center coordinate can also be quite different from the incoming coordinate (see Fig. 3). The final y coordinate can be a wild function of the initial conditions. As discussed in Section III, the scattering dynamics of abrupt potentials are *generic* and apply to potentials with finite gradients as well.

A special case that can be solved completely is scattering from a thin horizontal wall [9,10]. A portion of a scattering trajectory is shown in Fig. (4). For this case, the y guiding center coordinate is a constant of the motion, so that the interesting variable is the number of collisions. For a general hard scatterer, one can turn the continuous scattering trajectory into a discrete hamiltonian map, by recording only the points of collision with the scatterer. In general, this is a two-dimensional map, because both the collision point and contact angle are required to calculate the next collision point (and contact angle). For the thin horizontal wall, however, since the y guiding center coordinate is a constant of the motion, the hamiltonian map is one-dimensional.

The perimeter of the horizontal wall is parameterized by $x \in [0, 1]$. There are two dimensionless parameters, the diameter of the cyclotron orbit α, and the amount by which the

orbit translates in one period, equal to 2β, which is proportional to the Hall field $\vec{E}$. Both α and β are measured in units of the wall perimeter. There is also an initial condition, the angle $\theta \in [0, 2\pi)$ at which the particle begins with its guiding center a specified distance from the barrier.

The one-dimensional Hamiltonian map can be used to calculate the number of collisions N, maximized over the initial condition θ, for a given set of parameters. A fairly typical section through parameter space is shown in Fig. (5). For the largest r plotted (largest electric fields), the particle can collide no more than 5 times with the barrier. As the field is reduced, it becomes possible to collide 9 times, then 13. As r is reduced further, N diverges. (All of the spikes in Fig. (5) diverge to infinity, and appear finite only because of finite numerical sampling.) N falls, diverges again, and in fact diverges an infinite number of times before reaching an accumulation point ar $r = 3.5$. A simple analytic formula describes the location of the divergences. Other sets of divergences are found at still lower r.

As r approaches a typical point of divergence, the particle trajectory approaches a periodic trajectory, such as the one shown in Fig. (6). A scattering state coming from $-\infty$ cannot become caught in a strictly periodic trajectory. (One way to see this is that the time-reversed trajectory would be indeterminate—it cannot both exit to $-\infty$ and continue to be periodic.) A scattering state can, however, enter a trajectory that is arbitrarily close to a periodic trajectory. In that case, the trajectory corresponds to slightly mistuned parameters, so that the trajectory comes close to the periodic trajectory, but does not quite close.

Figure (7) plots the set of points in parameter space at which infinite trajectories exist. The periodic orbits occur on rays coming from the origin. As will be discussed below, there are also lines of *quasiperiodic* infinite orbits, such as the one extending upward and to the right from $(r, s) = (0.25, 0)$. The lines of periodic orbits are impaled on the lines of quasiperiodic orbits. The length of the periodic line segments is a discontinuous function of the distance along the quasiperiodic line.

One can construct an exact renormalization group (RG) description of the orbits. The RG is implemented by constructing first return maps of ever smaller intervals of the perimeter of the wall. The intervals must be chosen with care so that the map does not become more complicated at each stage. The existence of quasiperiodic infinite orbits is known because the corresponding fixed point of the RG is isomorphic to irrational rotations of a circle. Details of the RG are given in Ref. [9].

For a random initial condition, the amount of time spent in the vicinity of a scatterer has a power law distribution for long times. One then expects that as a particle encounters a succession of scatterers, $1/f^{\gamma}$ noise will result.

III. GENERAL POTENTIALS

The thin horizontal wall shows unusual scattering behavior in a magnetic field, including the existence of infinite orbits. It is important to know whether infinite orbits occur for general potentials in a magnetic field, or whether they are specific to the thin horizontal wall. It will be shown that infinite orbits occur in general, for both abrupt and smooth potentials.

The abrupt potential considered in this section is a general simple closed curve Λ, outside of which the potential $V(\vec{r})$ vanishes, and inside of which the potential is infinite (or equivalently, larger than the maximum kinetic energy of the particle). The curve Λ should be differentiable (have a unique tangent vector) almost everywhere, so that the scattering process is well defined. A particle whose trajectory intersects Λ reflects at the boundary, with the angle of incidence equal to the angle of reflection.

Consider an arbitrary initial position and momentum $(\vec{r}, \vec{p})$, as shown in Fig. (8). Somewhere along the trajectory, place a short reflecting line segment at an arbitrary angle. The particle collides, and another line segment is placed across a later part of the trajectory. This process is continued, and in most cases the trajectory will eventually intersect itself. The final line segment is placed through this intersection at an angle such that the angle of

incidence equals the angle of reflection. The final line segment is shaded with stripes. The full curve Λ can be any curve that passes through the points at which the collisions occur with a tangent vector parallel to the line segments.

Many potentials that have an infinite periodic trajectory for a given initial position and momentum have thus been constructed. The set of potentials is of co-dimension 2, since what is required is that the one-dimensional manifold Λ intersects a particular point with a particular slope (at the striped line segment). As before, by slightly mistuning the parameters (initial position, momentum, electric field, or magnetic field), a scattering state results that collides with the potential an arbitrarily large number of times before escaping to infinity.

We have also demonstrated a solution to a related problem: given a potential, to find an initial $(\vec{r}, \vec{p})$ that results in a periodic trajectory. This problem was solved analytically for rectangles [11]. One can also make the following observation for general abrupt potentials. Assume the magnetic field, the Hall field, and the potential are given. The initial conditions for a trajectory are the initial point along the perimeter, and the initial momentum vector given by $|\vec{p}|$ and θ_p. If the trajectory is to be periodic after one orbit, it must return to the the initial point with the correct contact angle. Since energy is conserved, $|\vec{p}|$ will be correct if the contact point is correct. There are 3 initial conditions and two equations to be satisfied. Usually (but not always) there will be a one-dimensional manifold of solutions.

The thin horizontal wall is known to have two classes of infinite trajectories, periodic and quasiperiodic. It is not known whether infinite trajectories that are not periodic exist for general potentials.

We now consider smooth potentials $V(\vec{r})$ that do not have abrupt walls, but rather may have a well-defined finite gradient everywhere. The following discussion does not apply to the special case in which V is infinitely slowly varying ($|\vec{\nabla} V|$ is infinitesimal everywhere), which results in trajectories that follow equipotential lines to arbitrarily good approximation.

Scattering from a smooth potential that has a finite gradient everywhere is compared with scattering from an abrupt potential in Fig. (9). It is clear that there is no important

qualitative difference between the two cases. For smooth potentials, the trajectory does not advance as far to the right. Comparable behavior then occurs in a shorter distance. The construction illustrated in Fig. (8) can be repeated with the reflecting line segments replaced by regions where V rises at a finite rate. It is simplest if the striped line segment at the self-intersection remains an abrupt reflecting wall. This wall can, however, be replaced by a region where V rises at a finite rate in the vicinity of the self-intersection. Periodic trajectories thus occur for smooth potentials as well.

IV. QUANTUM POTENTIAL SCATTERING

In the quantum problem, the radius of the cyclotron orbit is quantized. The allowed radii correspond to the Landau levels $n = 0, 1, 2, \ldots$. An electron has a second quantum number $\vec{k}$, which (in the Landau gauge) adjusts its y guiding center coordinate. An incident electron wavefunction $|n_1, \vec{k}_1>$ can scatter and emerge in state $|n_2, \vec{k}_2>$. Since energy is conserved in the collision, for each outgoing Landau level index n_2, only one guiding center momentum k_2 is allowed. For example, suppose the Landau level index is increased by 1 in the collision, increasing the particle's kinetic energy by $\hbar\omega_c$. Then $\vec{k}$ must change by an amount such that the y guiding center coordinate moves downhill in the Hall electric field $\vec{E}$, lowering the potential energy by $\hbar\omega_c$.

Quantum scattering is described by a scattering matrix that gives both the amplitude and the phase to scatter into a given Landau level. An incident electron that develops a substantial amplitude to scatter into a higher Landau level, for example as $\vec{E}$ is increased, signals the breakdown of the quantum Hall effect. Because the y guiding center changes, the collision induces a component of the current in the direction of the electric field, or a nonzero diagonal conductivity $\sigma_{yy} = \sigma_{xx}$. A conductivity σ_{xx} that increases rapidly with E is an experimental sign of the breakdown of the QHE [12].

The phase of the scattering matrix contains information on the displacement of a wavepacket in the $\hat{x}$ direction compared to its position if the potential were zero. The dis-

placement is proportional to $-\partial\phi/\partial E$, where the energy E is proportional to $\vec{k}$ (and to the y guiding center coordinate). Thus, a rapid change in $\phi(E)$ can signal that the wavepacket is getting caught in a resonance, which is the quantum equivalent of a long classical orbit.

The quantum scattering effects of interest cannot be calculated by perturbing in the potential $V(\vec{r})$ or in the Hall field $\vec{E}$, nor are they given by methods such as the self-consistent Born approximation [13]. We have used two methods for quantum scattering. The first is an exact transfer matrix method applied to a lattice that is finite in the $\hat{y}$ direction and infinite in the $\hat{x}$ direction. The second is a quasiclassical Wigner density functional approximation. The quasiclassical method uses Wigner's definition to calculate the phase space density $f(\vec{r},\vec{p},t=0)$ from the incoming wavefunction Ψ_1. The density f is then numerically time evolved ***classically*** until essentially the entire ensemble has escaped from the scatterer. The resulting distribution $f(\vec{r},\vec{p},t)$ is projected back onto an outgoing wavefunction Ψ_2, which defines a scattering matrix. The two methods of calculating quantum scattering are compared. In cases where there is close agreement, one can conclude that the quantum dynamics is essentially following the classical dynamics. For more details about these methods and the results obtained, see Refs. [14,15,11].

A quantum wavepacket encountering a very slowly varying potential has behavior quite similar to the classical case [5–8]. The Landau level index never changes. The only modification required in Fig. (2) is that now a wavepacket follows guiding center trajectory. In the direction perpendicular to the local guiding center trajectory, the wavefunction for the ground Landau level is a gaussian of extent equal to a magnetic length $l=\sqrt{\hbar c/eB}$. Near a saddle point, the wavepacket can split, and follow two different trajectories with substantial amplitude.

We now consider the relationship of quantum and classical dynamics for an abrupt potential. The (quantum) phase shift ϕ for typical scattering from an abrupt potential is shown in Fig. (10). The additional displacement Δx of a wavepacket due to the potential is proportional to $-\partial\phi/\partial E$. The plot shows that the potential generally speeds the electron's

progress in the $\hat{x}$ direction, except at a resonance in the vicinity of energy $E = 1.14$, where the electron is slowed down significantly. Figure (11) shows the number of collisions N for *classical* scattering with parameters that have large weight in the corresponding Wigner density functional near the resonance. It can be seen that long classical orbits occur. (We have demonstrated analytically that infinitely long classical orbits occur, which appear finite in Fig.(11) because of finite numerical sampling.) The long classical trajectories circle the scatterer many times, as shown in Fig. (12). In contrast, the very short trajectories, which are more common, are deflected above the scatterer and immediately escape for the parameters of Fig. (11). The short trajectories do not orbit, and thus have no classical probability of being immediately below the scatterer.

This observation suggests that the relationship of quantum to classical scattering can be further tested by calculating the probability that the electron is immediately below the scatterer divided by the probability that it is immediately above the scatterer for the exact quantum eigenstate. Figure (13) shows that this probability is sharply peaked at the center of the quantum resonance at $E = 1.14$. Thus quantum mechanically as well, a resonance occurs when the electron orbits the scatterer many times before escaping. Also shown in Fig. (13) is that there is an enhanced probability of scattering into another Landau level at the center of the resonance.

Figure (14) shows the probability of scattering into the same (0) and higher (1) Landau levels for an abrupt rectangular scattering potential. The quasiclassical calculation gives a semiquantitative approximation to the exact result. It does, however, overestimate the amount of scattering out of the ground Landau level at low fields $\vec{E}$.

The calculation of phase shifts using the quasiclassical method is more difficult than the calculation of scattering amplitudes. Phase shifts signify time delays that have to be resolved by considering the behavior of superpositions of eigenstates with a finite energy difference. This calculation can be done by classically evolving Wigner distributions corresponding to such superpositions, and in the case of not too large phase shifts shows semiquantitative agreement with the exact phase shifts [14,15,11].

There are some parallels to the potential scattering investigated here and 4 terminal junction behavior. Classical and quantum transmission of electrons through 4 terminal junctions is calculated in Refs. [16–18]. The first two of these references consider the behavior in magnetic fields.

V. BREAKDOWN OF THE QUANTUM HALL EFFECT

The first experiments on the breakdown of the quantum Hall effect were published in the early 1980's [12]. In this section, we compare theoretical predictions to some careful recent experiments by Kawaji et al. [19].

Consider an electron that encounters a scattering potential of extent L_0 in the y-direction, and scatters into a higher Landau level, leading to the breakdown of the QHE. The maximum total distance it can scatter in the y-direction is approximately $L = L_0 + y_1 + y_2$, where $y_1 = l\sqrt{2n+1}$ is the width of the incoming wavepacket in Landau level $n = 0, 1, 2, \ldots$, and $y_2 = l\sqrt{2n+3}$ is the width of the outgoing wavepacket in the next Landau level (see Fig. 15). This formula has been verified by simulations for moderate L_0. The breakdown electric field E is obtained by setting $eEL = \hbar\omega_c$, which results in

$$E = \frac{\hbar B}{mc[L_0 + l(\sqrt{2n+1} + \sqrt{2n+3}\ )]}. \tag{5.1}$$

If there are several scatterers with differing widths in the sample, the largest L_0 should be used in Eq. (5.1) to give the observed breakdown field. When the range L_0 of the scatterer vanishes, Eq. (5.1) reduces to the equation that Kawaji et al. use for point scatterers [19,20].

As can be seen from Fig. (16), the theoretical breakdown field using point scatterers is substantially larger than the measured breakdown field. The field dependence of the point scattering theory is also too large. A satisfactory fit to the experimental data can be obtained by assuming extended scatterers and setting the only free parameter in Eq. (5.1) to $L_0 = 1.1\mu m$. The overall magnitude is obtained by a suitable choice of L_0. The weaker field dependence is also correctly obtained. Kawaji et al. propose the test of fitting E/E_{pst}

for $i = 2$ divided by the value at $i = 1$, where E_{pst} is the breakdown field that would be predicted from point scattering theory. The theoretical value from Eq. (5.1) is 2.1, which is not too far from the measured value of 2.5.

As discussed by Kawaji et al., no other quantitative theory can explain their data. The authors propose a qualitative theory involving the ratio of extended to localized states. If at some point quantitative predictions are to be made based on this idea, it should be taken into account that this ratio is a highly singular function of the electric field [5], and must be calculated self-consistently.

VI. SUMMARY

We have shown that classical potential scattering in a magnetic field is complex, and exhibits resonances in which an arbitrarily large number of collisions can occur. This applies not only to a hard wall potential that can be solved completely, but also for generic scattering potentials with finite gradients. Only infinitely slowly varying potentials are in a class by themselves, with trivial scattering dynamics for trajectories that do not approach saddle points. Quantum scattering follows the classical dynamics rather closely, and shows sharp quantum resonances. We have also shown that extended scatterers can cause the QHE to break down at much weaker fields than can point scatterers. This theory provides the only viable quantitative explanation (so far) of the recent breakdown of experiments of Kawaji et al. [19].

Some open questions include: (1) Finding a quantitative description for the change in guiding center coordinate and the number of collisions for general potentials. (2) Determining whether nonperiodic classical bound states exists for general potentials. (3) Calculating the exponent for $1/f^{\gamma}$ noise for both the horizontal wall and for general potentials. (4) A more detailed comparison to experiments measuring noise and fluctuation effects.

This work was supported by the US Department of Energy.

REFERENCES

[1] *The Quantum Hall Effect*, edited by R. E. Prange and S. M. Girvin (Springer-Verlag, New York, 1987).

[2] *Quantum Hall Effect*, edited by Michael Stone (World Scientific, New Jersey, 1992).

[3] A. Karlhede, S. A. Kivelson, and S. L. Sondhi, *The Quantum Hall Effect: The Article*, Lectures presented at the 9th Jerusalem Winter School on Theoretical Physics, January 1992.

[4] R. B. Laughlin, Phys. Rev. B **23**, 5632 (1981).

[5] S. A. Trugman, Phys. Rev. B **27**, 7539 (1983).

[6] R. E. Prange and R. Joynt, Phys. Rev. B **25**, 2943 (1982).

[7] S. V. Iordansky, Solid State Commun. **43**, 1 (1982).

[8] R. F. Kazarinov and S. Luryi, Phys. Rev. B **25**, 7626 (1982).

[9] S. A. Trugman, Phys. Rev. Lett. **62**, 579 (1989).

[10] S. A. Trugman and F. R. Waugh, Surf. Sci. **196**, 171 (1988).

[11] V. Nikos Nicopoulos, Ph.D. Thesis, Princeton University, 1990 (unpublished).

[12] M. E. Cage *et al.*, Phys. Rev. Lett. **51**, 1374 (1983). G. Ebert *et al.*, J. Phys. C **16**, 5441 (1983).

[13] The self-consistent Born approximation has shortcomings even for linear response; see T. Ando, Y. Matsumoto, and Y. Uemura, J. Phys. Soc. Japan **39**, 279 (1975).

[14] V. Nikos Nicopoulos and S. A. Trugman, Phys. Rev. Lett. **65**, 779 (1990).

[15] V. Nikos Nicopoulos and S. A. Trugman, Phys. Rev. B. **45**, 11004 (1992).

[16] C. W. J. Beenakker and H. van Houten, Phys. Rev. Lett. **63**, 1857 (1989).

[17] H. U. Baranger and A. D. Stone, Phys. Rev. Lett. **63**, 414 (1989); H. U. Baranger, D. P. DiVencenzo, R. A. Jalabert, and A. D. Stone, Phys. Rev. B **44**, 637 (1991).

[18] M. L. Roukes and O. L. Alerhand, Phys. Rev. Lett. **65**, 1651 (1990).

[19] S. Kawaji, K. Hirakawa, M. Nagata, T. Okamoto, T. Fukase, and T Gotoh, J. Phys. Soc. Japan **63**, 2303 (1994).

[20] D. C. Tsui, G. J. Dolan, and A. C. Gossard, Bull. Am. Phys. Soc. **28**, 365 (1983).

FIGURES

FIG. 1. Potential scattering in zero magnetic field.

FIG. 2. Scattering from a smooth potential in a magnetic field, for which two equipotential surfaces are shown. The guiding center trajectory is shown as a heavy line. A portion of the full trajectory is shown on the left.

FIG. 3. Scattering from a hard square.

FIG. 4. Scattering from a thin horizontal wall.

FIG. 5. The number of collisions N maximized over initial angle θ as a function of $r = \alpha + \beta$, with $s = \alpha - \beta$ fixed at 0.2. N is plotted on a log scale.

FIG. 6. A periodic trajectory is shown as a heavy line. For slightly mistuned parameters, the trajectory does not quite close (light line), and eventually escapes.

FIG. 7. The set of parameters for which infinite trajectories exist. Plotted parameters are of the form $(r, s) = (j_1/p, j_2/p)$, with j_1 and j_2 integers and $p = 2520$. Figure (5) is taken on the horizontal section $s = 0.2$.

FIG. 8. The trajectory starts near the tail of the arrow. The short, heavy line segments are arbitrary reflecting walls. To obtain a periodic trajectory, the final reflecting wall (striped) must be placed at the self- intersection point at the correct angle. A curve Λ that supports this periodic trajectory can be any curve that passes through the line segments with a tangent parallel to the line segment.

FIG. 9. A trajectory that collides with a hard wall is shown above, and with a smoothly rising potential below. The potentials are nonzero inside of the shaded regions.

FIG. 10. Scattering phase shift for a free eigenstate encountering a rapidly varying potential that is strongly repulsive inside a rectangle. The phase shift is given for both the incoming and outgoing states in the first excited Landau level. The energy is proportional to the y guiding center coordinate.

FIG. 11. Long classical orbits occur in parts of the region shown, with radius r plotted between 1.308 and 1.312, and the incoming phase ϕ between 2.337 and 2.339.

FIG. 12. A portion of a long classical trajectory occurring in Fig. (11) is shown.

FIG. 13. The probability for finding the electron directly below the scatterer divided by the probability for finding it above in the exact quantum eigenstate (squares, left scale). The probability of scattering into the second Landau level is shown by circles, right scale.

FIG. 14. Scattering probability of a ground Landau level (0) wave packet as a function of the Hall electric field. The solid lines are the results of the exact quantum calculation and the dashed lines are the results of the quasiclassical approximation. The probabilities for scattering into Landau levels higher than 1 are not shown.

FIG. 15. A wavepacket scatters from an extended object into the next Landau level, resulting in the breakdown of the quantum Hall effect.

FIG. 16. Experimental magnetic field dependence of the average critical electric field F_{cr}. The open squares are the theoretical prediction for point scatterers. The solid line is the present theoretical prediction for extended scatterers. Except for the solid line, this figure is taken from Kawaji et al. [19].

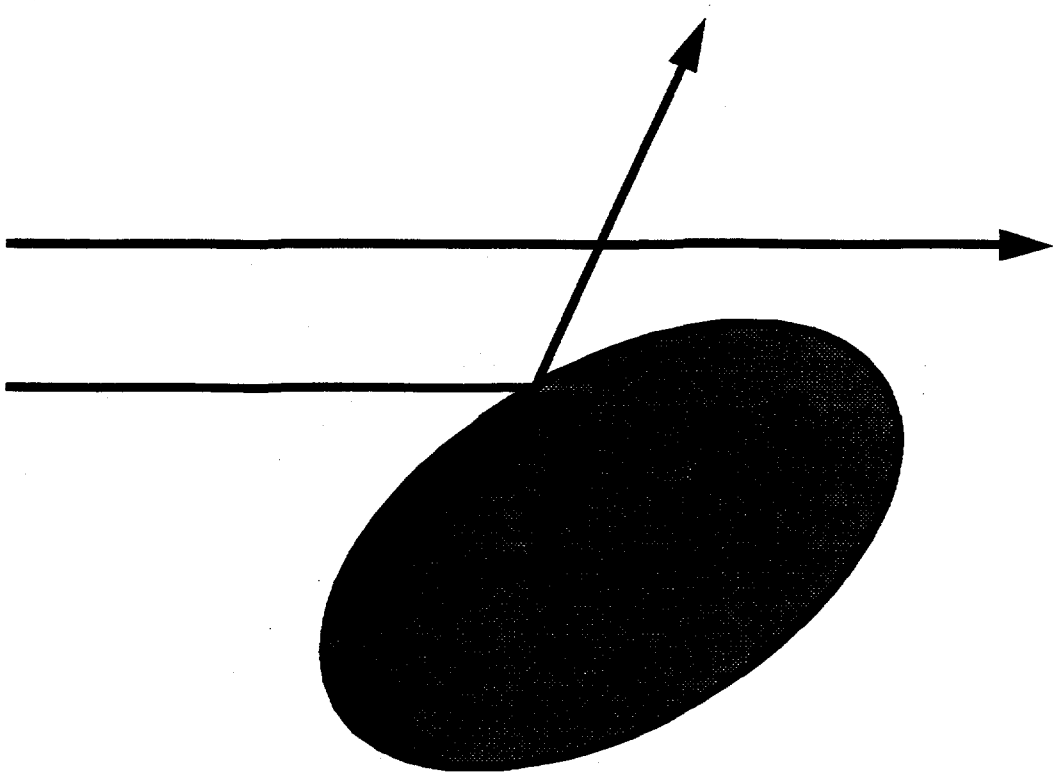

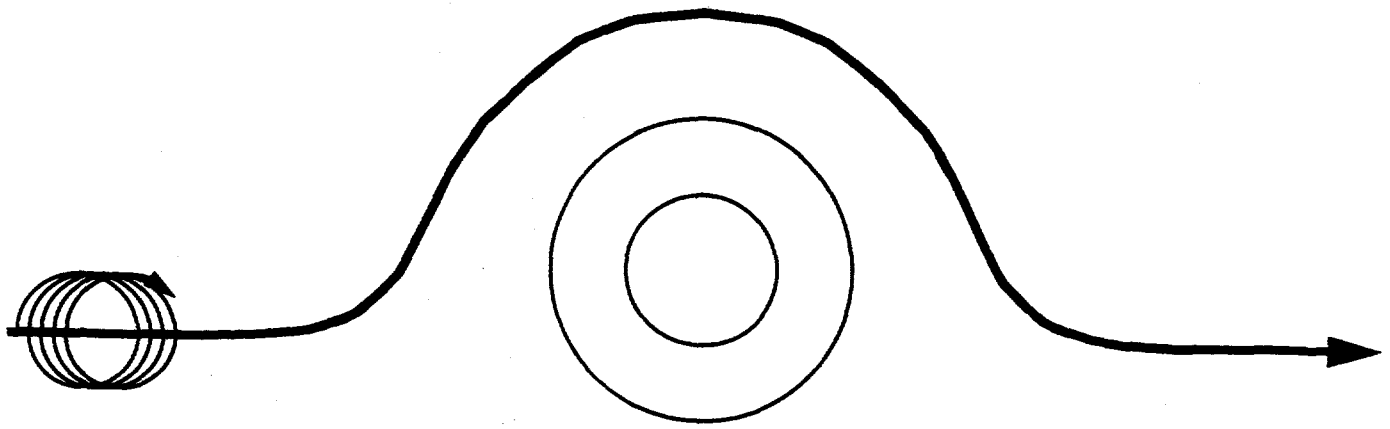

Trugman, Fig. 3

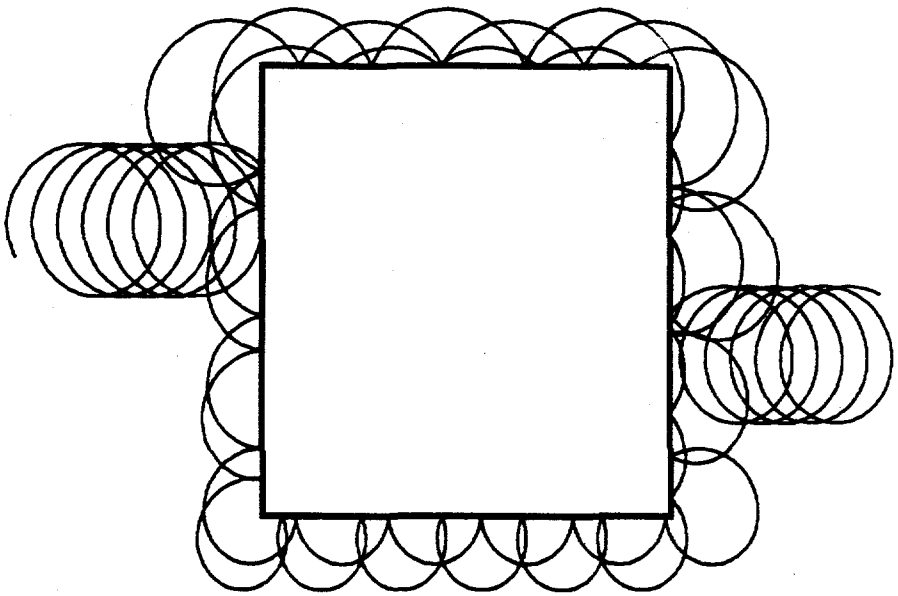

Trugman, Fig. 3

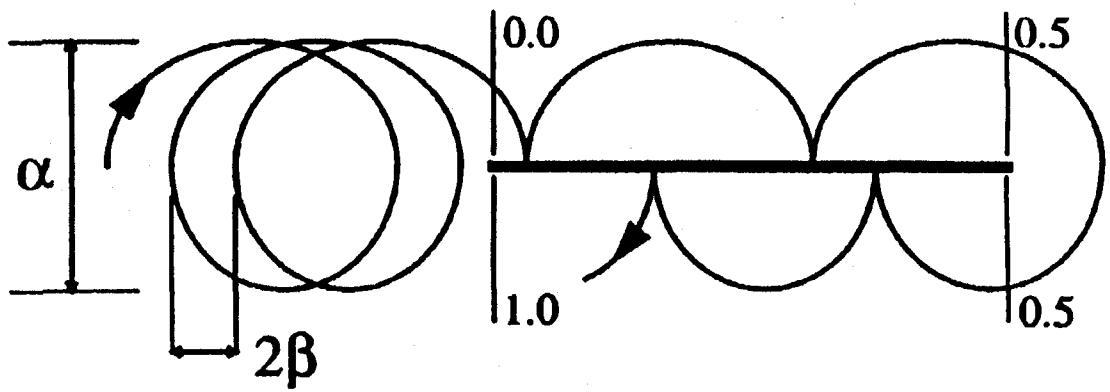
α
2β
0.0
1.0
0.5
0.5

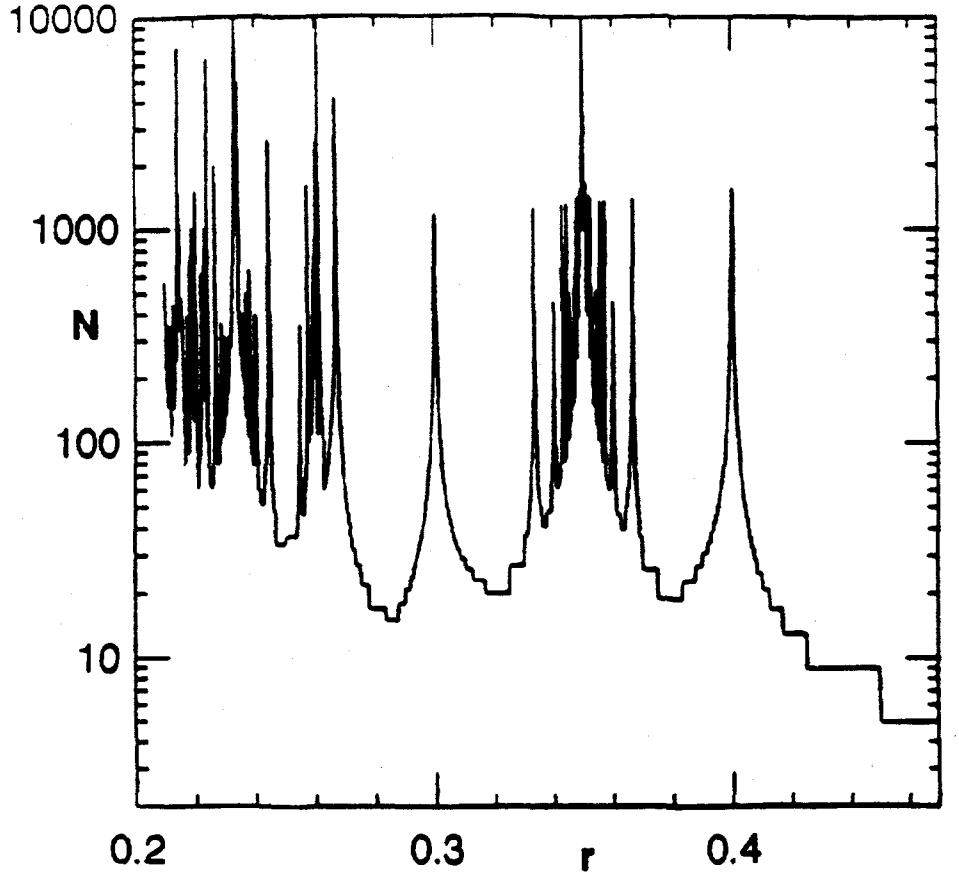

Trugman Fig. 5

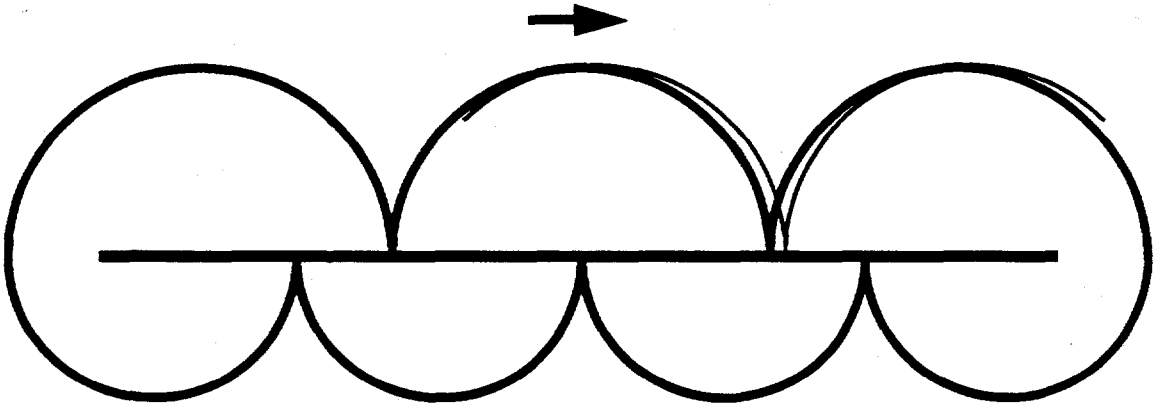

Trugman. Fig 6

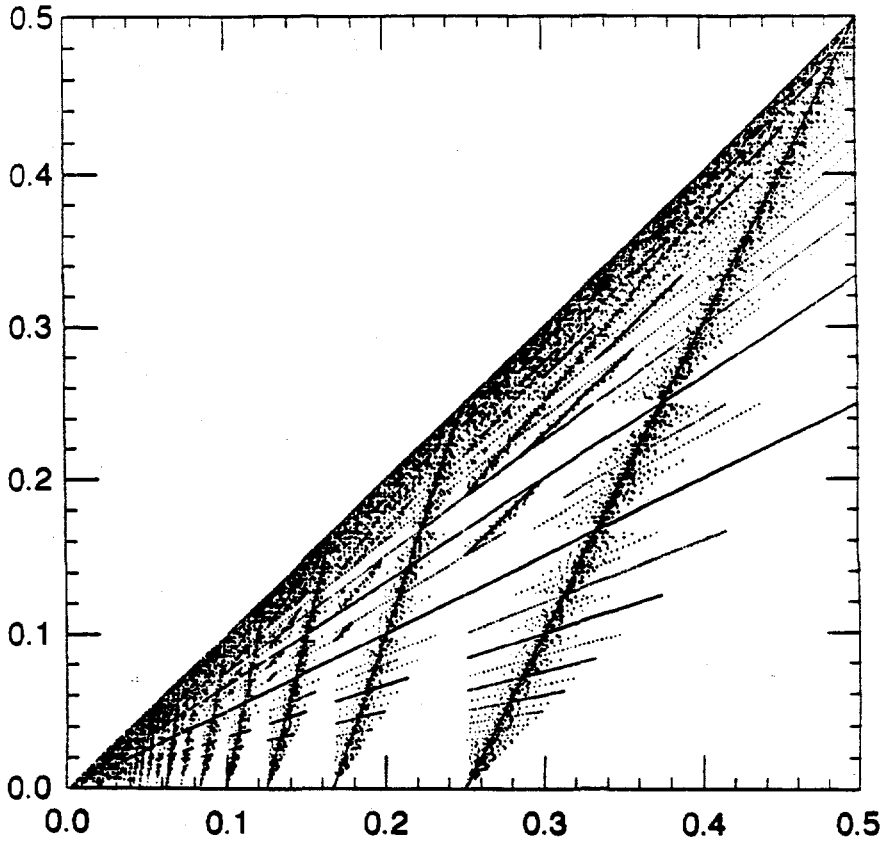

Trugman Fg. 7

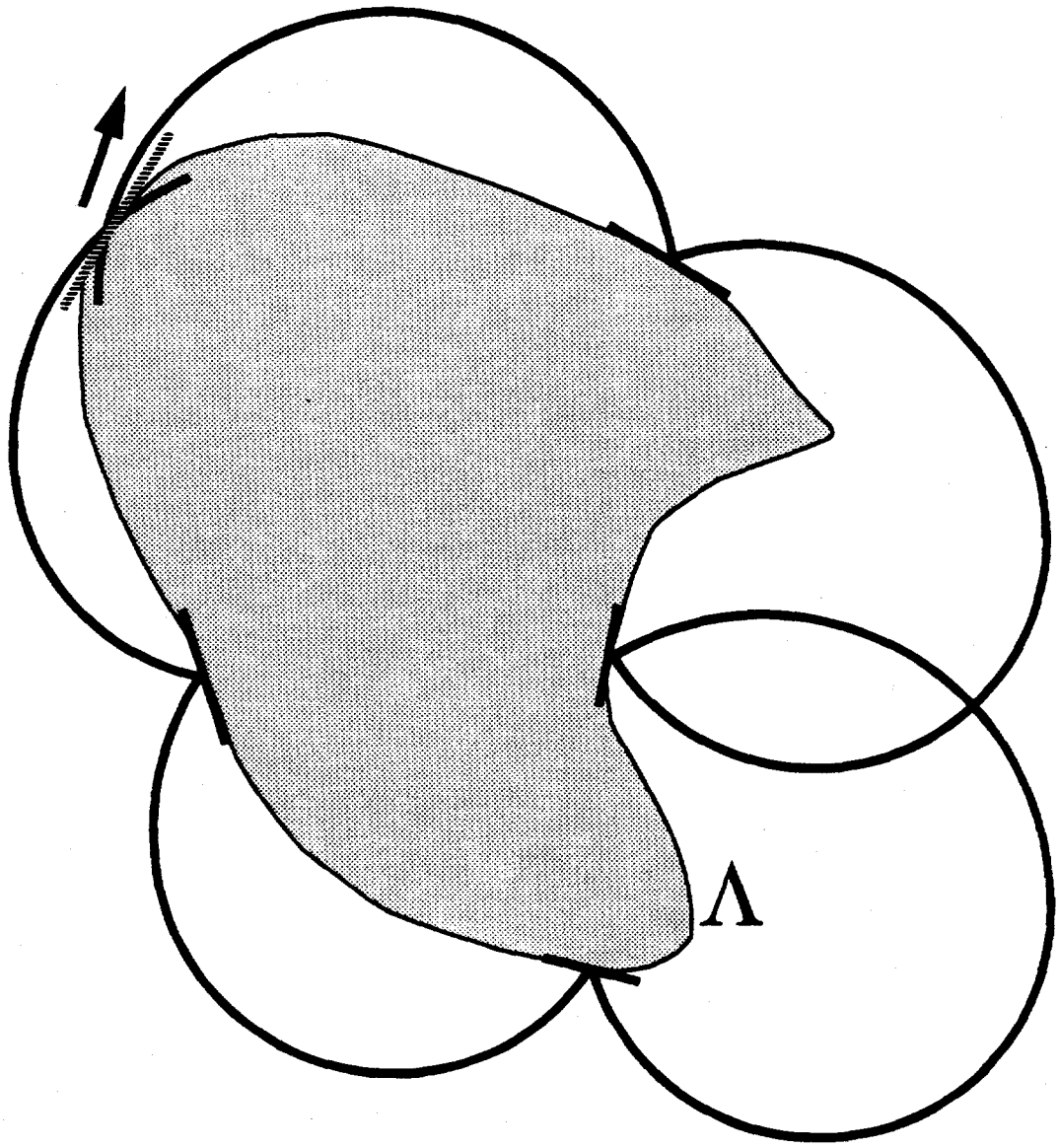

Trugman, E.g. 3

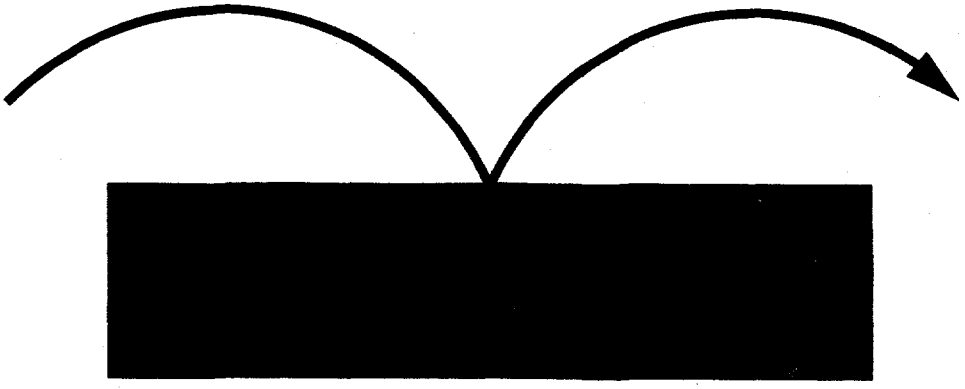

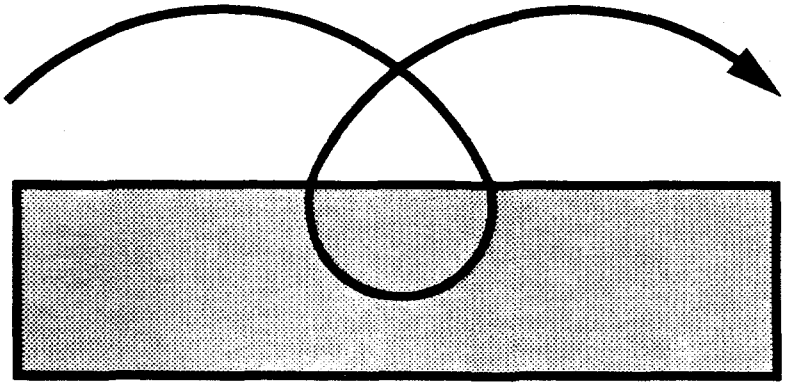

Trugman Fig. 7

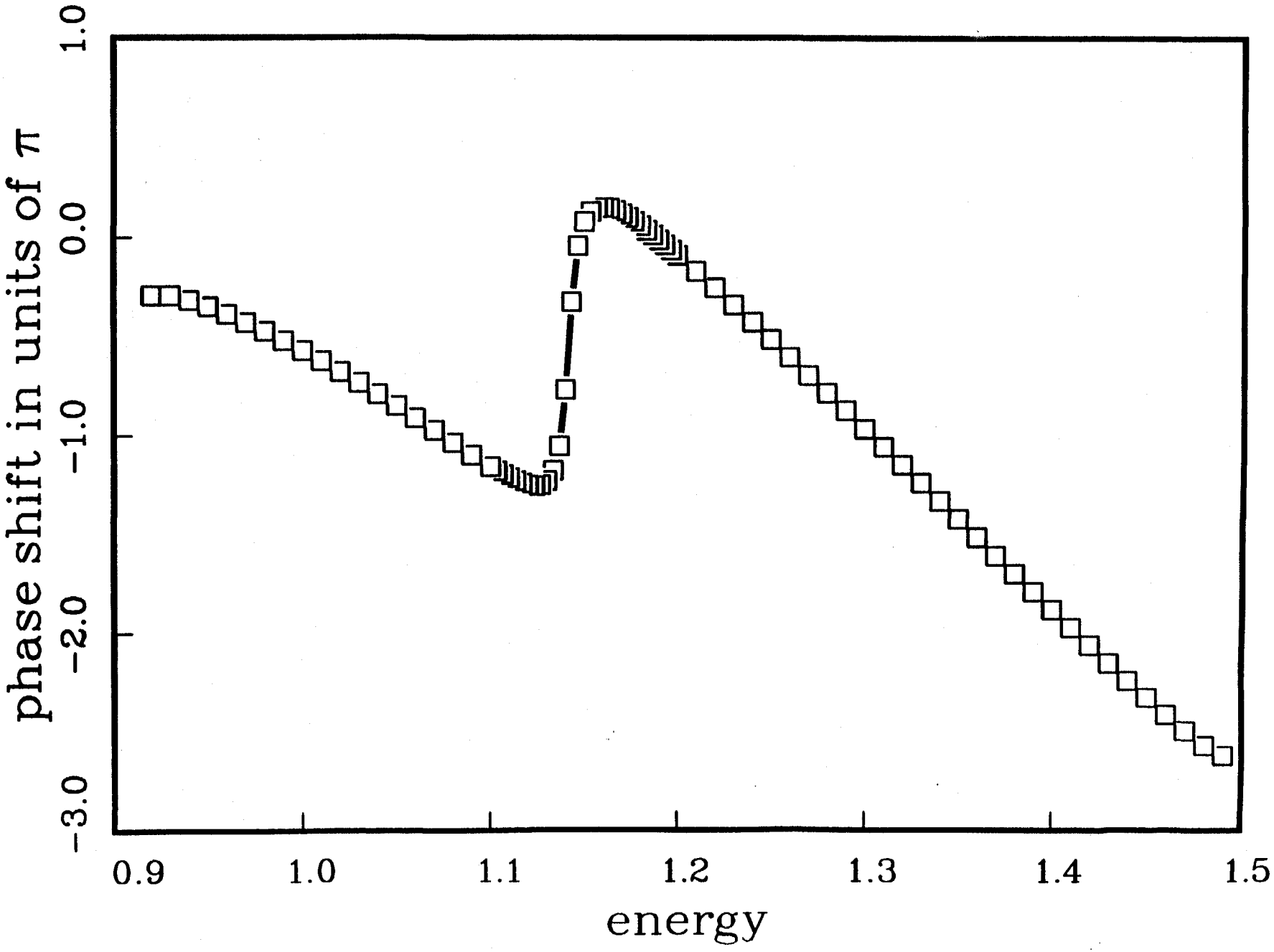
phase shift in units of π
1.0
0.0
−1.0
−2.0
−3.0
0.9
1.0
1.1
1.2
1.3
1.4
1.5
energy

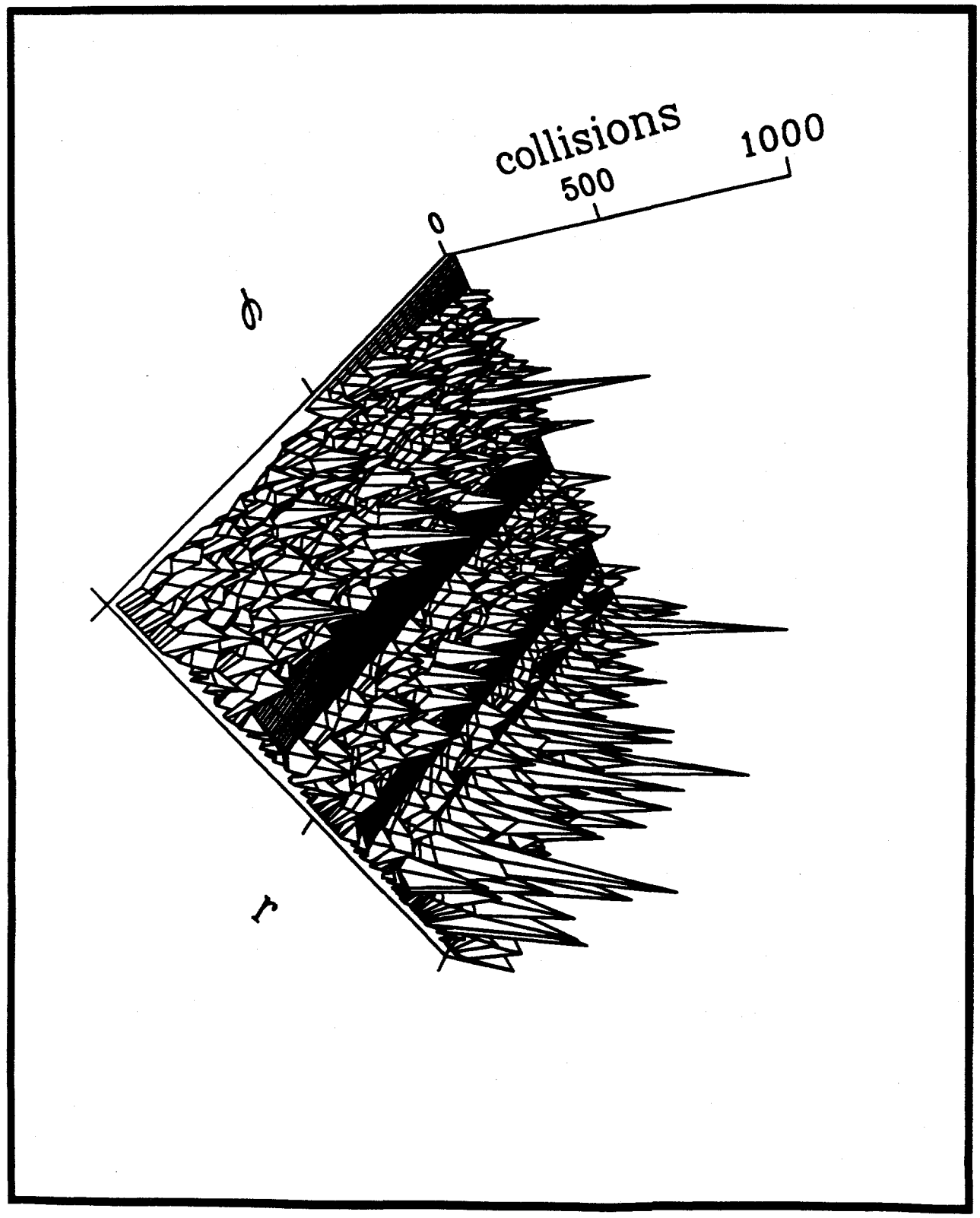
collisions
0
500
1000
ϕ
r

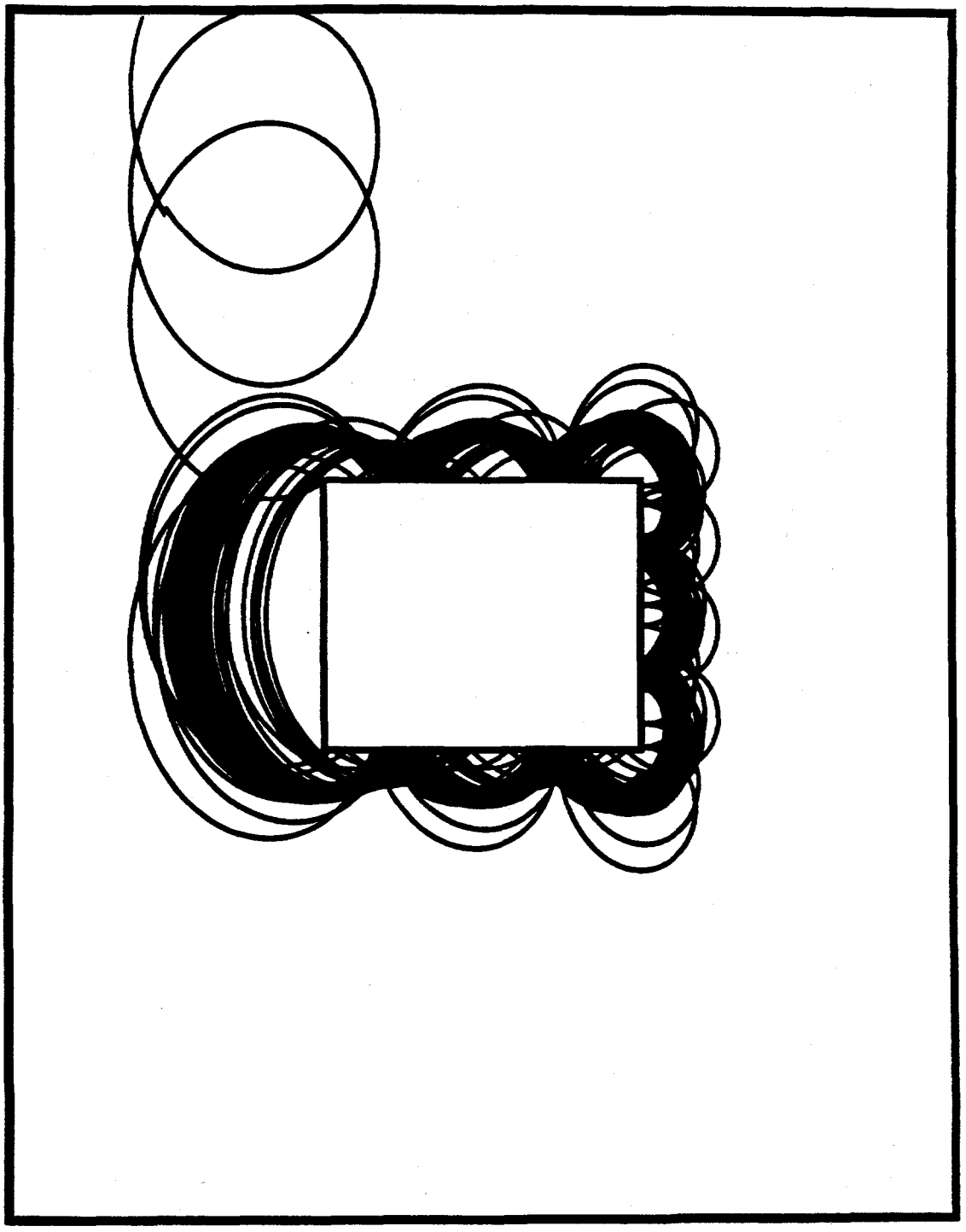

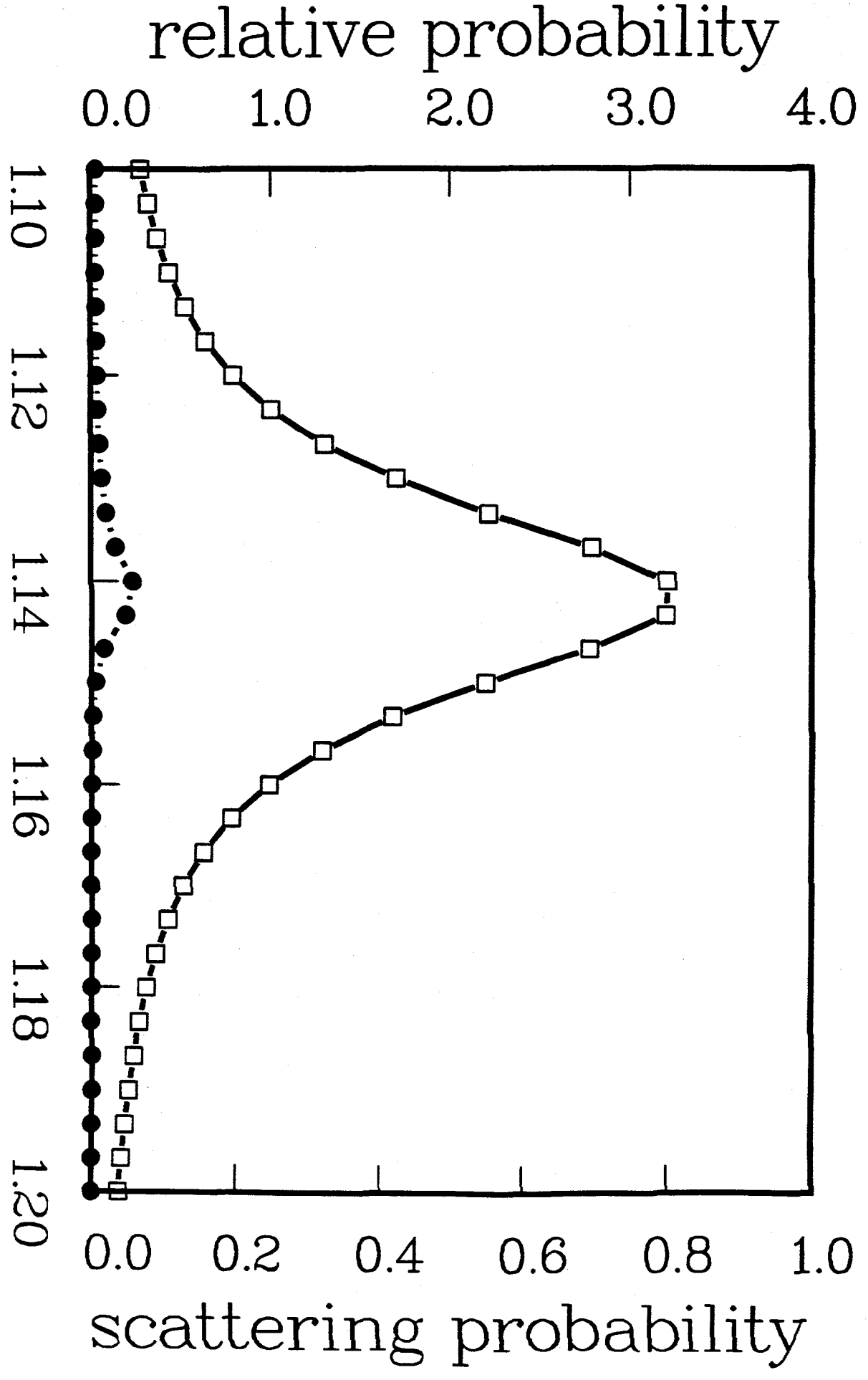
relative probability
0.0
1.0
2.0
3.0
4.0
1.10
1.12
1.14
1.16
1.18
1.20
0.0
0.2
0.4
0.6
0.8
1.0
scattering probability

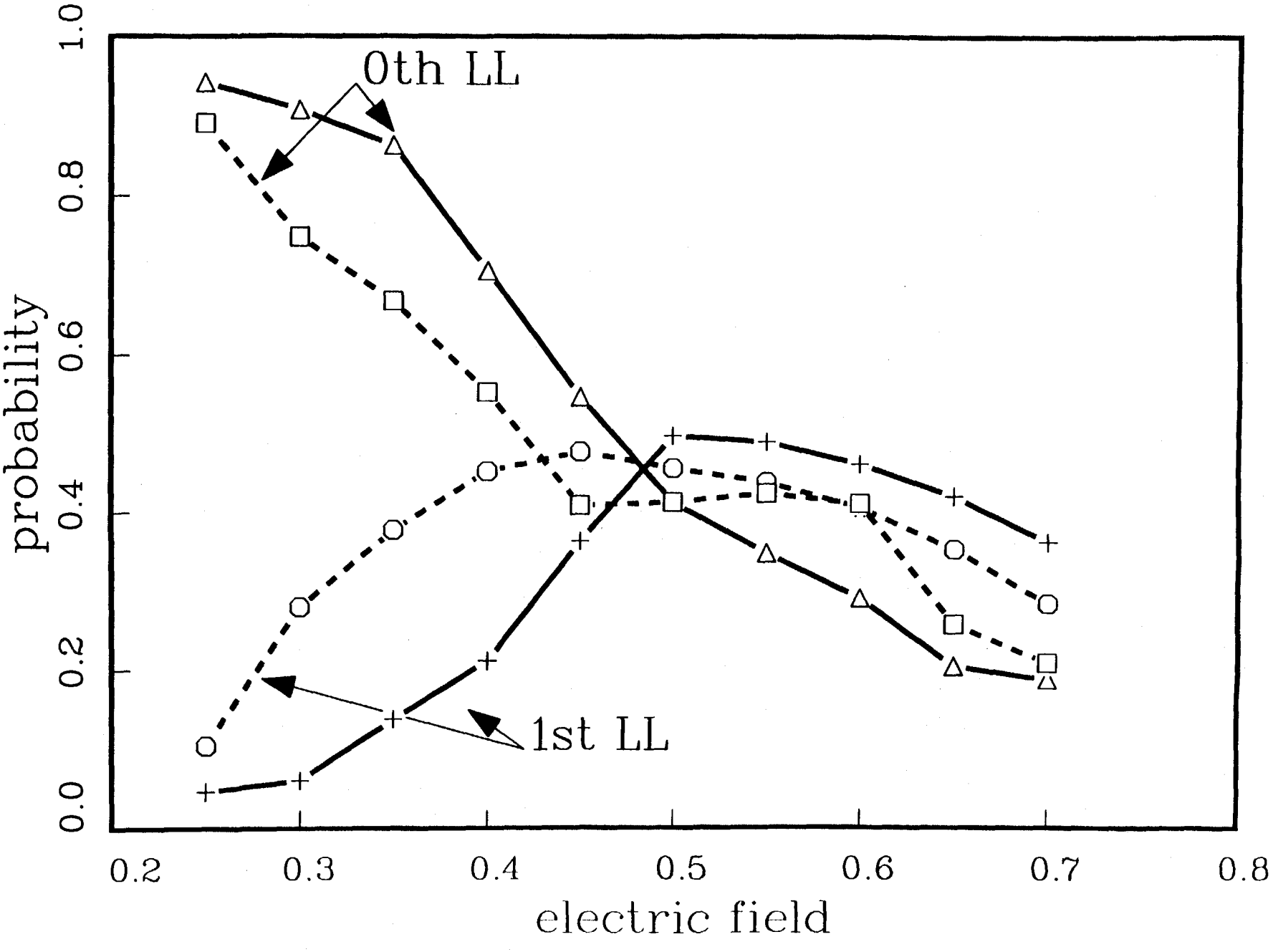
0th LL
1st LL
probability
electric field
0.0
0.2
0.4
0.6
0.8
1.0
0.2
0.3
0.4
0.5
0.6
0.7
0.8

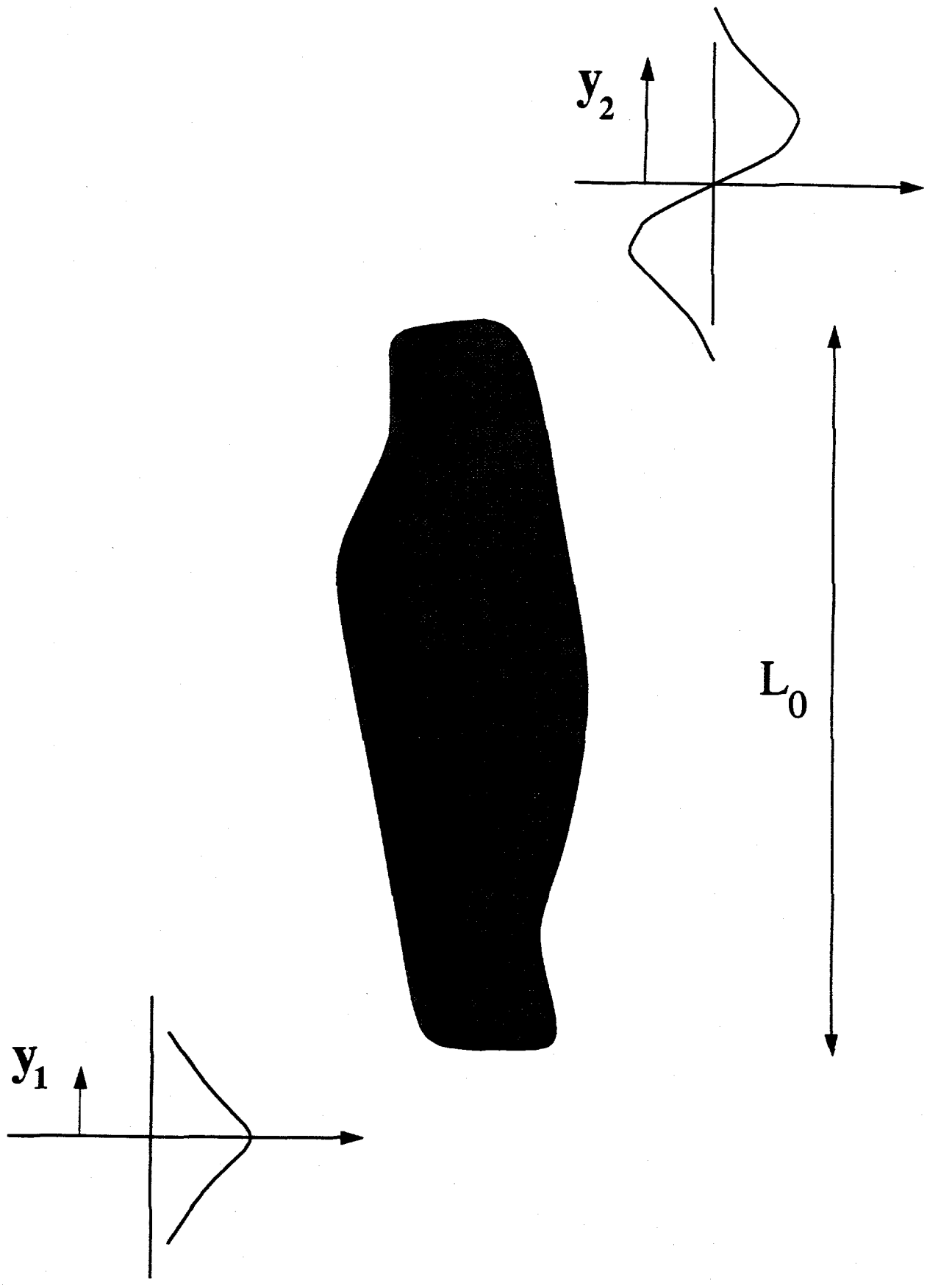

Trugman Fig 5

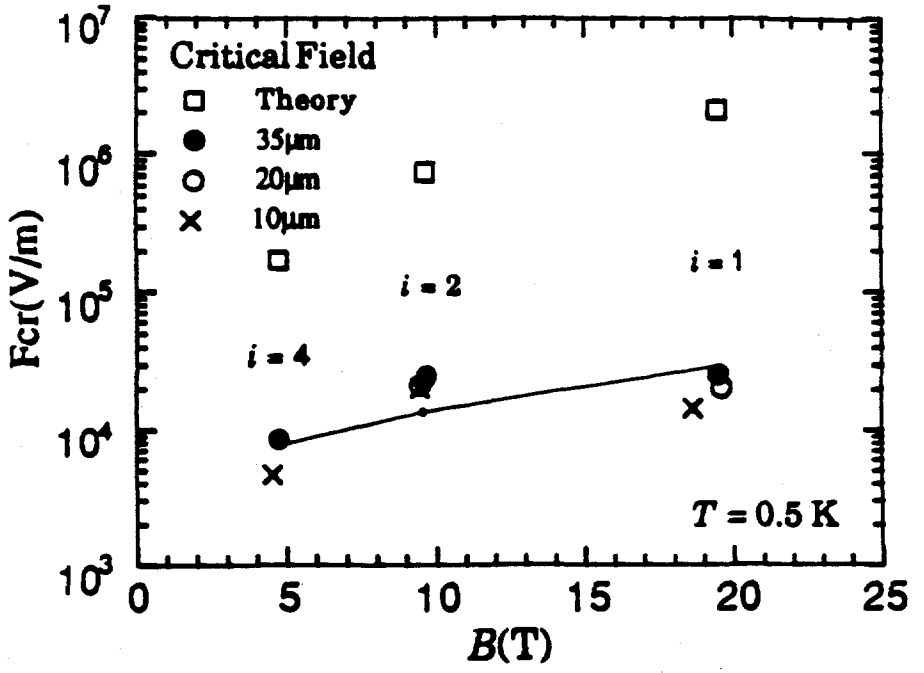

Trugman Fig 16